

Mechanism of Environmentally-Induced Stress Corrosion Cracking of Zr-Alloys

Sang Yoon Park[†], Jun Hwan Kim, Byung Kwon Choi, and Yong Hwan Jeong

Advanced Core Materials Lab, Korea Atomic Energy Research Institute
150 Doekjin-dong, Yuseong-gu, Daejeon, 305-353, South Korea

Iodine-induced stress corrosion cracking (ISCC) properties and the associated ISCC process of Zircaloy-4 and an Nb-containing advanced nuclear fuel cladding were evaluated. An internal pressurization test with a pre-cracked specimen was performed with a stress-relieved (SR) or recrystallized (RX) microstructure at 350 °C, in an iodine environment. The results showed that the K_{ISCC} of the SR and RX Zircaloy-4 claddings were 3.3 and 4.8 MPa · m^{0.5}, respectively. And the crack propagation rate of the RX Zircaloy-4 was 10 times lower than that of the SR one. The chemical effect of iodine on the crack propagation rate was very high, which was increased 10⁴ times by iodine addition. Main factor affecting on the micro-crack nucleation was a pitting formation and its agglomeration along the grain boundary. However, this pitting formation on the grain-boundary was suppressed in the case of an Nb addition, which resulted in an increase of the ISCC resistance when compared to Zircaloy-4. Crack initiation and propagation mechanisms of fuel claddings were proposed by a grain boundary pitting model and a pitting assisted slip cleavage model and they showed reasonable results.

Keywords : Iodine-induced stress corrosion cracking (ISCC), Zircaloy-4, Crack initiation, propagation, Threshold stress-intensity factor (K_{ISCC}), grain boundary pitting

1. Introduction

The presence of corrosive fission products can cause environmentally assisted cracking (EAC) of the nuclear fuel cladding tubes. The EAC phenomenon triggered by iodine is called as an iodine-induced stress-corrosion cracking (ISCC). Since the power of a LWR is frequently changed in load following operation, the possibility of releasing a fission-product gas becomes so large that SCC tends to increase. Nowadays, most of the nuclear power reactors are adopting a high burn-up to increase the fuel economy, where the refueling cycle of the fuel bundles is extended. As the fuel burn-up is going up, the diameter of the cladding is decreased, while the outer diameter of the fuel pellet is increased, the pellet and the cladding contact each other. Because the concentration of the iodine inside the fuel rod also gradually increases to cause SCC, The possibility of both mechanical and chemical interaction increased.¹⁾⁻³⁾

The nucleation and the propagation of an ISCC crack is very complex to be enough understood. It has been reported that the crack nucleation sites are; (a) intermetallic

and inclusion particles,⁴⁾ (b) intergranular sites,⁵⁾ (c) pits and flaws,⁶⁾ (d) hydrides⁷⁾ and (e) transgranular sites.⁸⁾ Prior to the crack propagation, the cladding has a long incubation time for an incipient crack to grow into a micro-crack. If the size of the micro-crack is large enough so that the stress intensity around a crack tip exceeds a threshold value, threshold stress-intensity factor (K_{ISCC}), the crack starts to propagate in a pseudo-cleavage mode and makes the cladding to be ruptured finally. Although the whole ISCC process has been proposed, the mechanism of a crack initiation and its growth is still far from being clearly understood.⁹⁾ A localized micro-void coalescence model was proposed,¹⁰⁾ but the evidence of the microductility on the fractured surfaces was not found.¹¹⁾ Some authors have associated pre-existing defects with the crack initiation sites in a fuel cladding,¹²⁾ but this has not been proven by experimentally.

In spite of many hypotheses and experimental results, little consensus has been made on a crack nucleation, not to mention of the intergranular or transgranular nature of a crack initiation. Recently, it has been proposed that the grain-boundary pitting coalescence (GBPC) and pitting-assisted slip cleavage (PASC) models are appropriate for modeling a crack nucleation and growth in a fuel

[†] Corresponding author: nsypark@kaeri.re.kr

cladding.¹³⁾ This study is aimed to evaluate these models by using the internal pressurization test under an iodine environment as well as detailed observations of the fractured surfaces on the tested cladding tube. These models are being reviewed with a Zircaloy-4 cladding tube, along with an Nb-contained zirconium cladding.

2. Experimental procedure

The specimens for this study were cut from a commercial grade low-tin Zircaloy-4 (Zr-1.3Sn-0.2Fe-0.1Cr) and Nb-contained Zirconium cladding (Zr-1.0Nb-1.0Sn-0.1Fe). Their outer and inner diameters were 9.50 mm and 8.36 mm, respectively. Their length was 130 mm. They were all as-received ones in a stress-relieved condition. To investigate the effect of the heat-treatment, the specimen was heat treated at 620 °C for 3 hours to have the fully recrystallized structure then it was also used for the ISCC test. The specimen having an initial crack inside the surface was used in the test. The pre-crack was created by the fatigue cracking method which Lemaignan¹⁴⁾ employed. A sine wave having 0.12 mm displacement and 5 Hz frequency, was applied to the specimen for the generation of an artificial crack at a depth of 25~50% inside its thickness.

Test specimen was put inside the autoclave, and then the medium, which was mixed with pure argon iodine, was pressurized inside the cladding after reaching a constant test temperature of 350 °C. The iodine used in this study, which had a purification of 99.99%, was supplied by Aldrich. With the exception of concentration variation tests, the iodine concentration was kept constant at 1.5 mg/cm². To minimize oxidation at the outer surface, the autoclave was evacuated then filled with argon gas before each test. The test was stopped either when a leakage oc-

curred around the test specimen or, if the specimen did not leak, after 100 reaching hours. After the test, the specimen was examined using optical microscope (OM) and scanning electron microscope (SEM) to determine the actual crack propagation depth during the ISCC test, and then the crack propagation velocity was evaluated. ISCC crack velocity with respect to the applied K_I was evaluated to determine the threshold stress intensity factor (K_{ISCC}). The K_I value was adjusted so that the stress state round the crack tip could be a plane strain condition.

3. Results

Fig. 1 shows the schematic crack shape, crack propagation mode and SEM fractographs of the fully recrystallized (RX) Zircaloy-4 specimen which was pre-cracked and pressurized at 145 MPa for 12.3 hr in the iodine

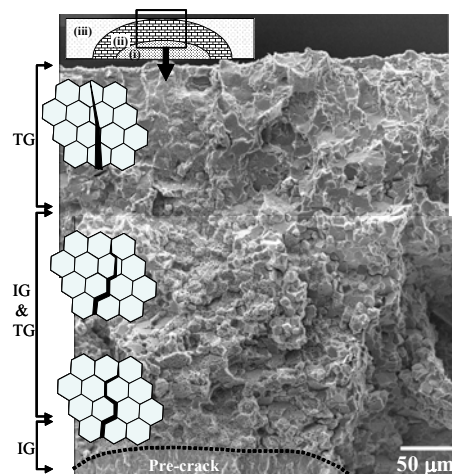


Fig. 1. Fractographs of an ISCC crack for Zircaloy-4 (RX) cladding pressurized in an iodine environment at 350 °C; (i) Fatigued pre-crack, (ii) ISCC (iii) ductile fracture after test.

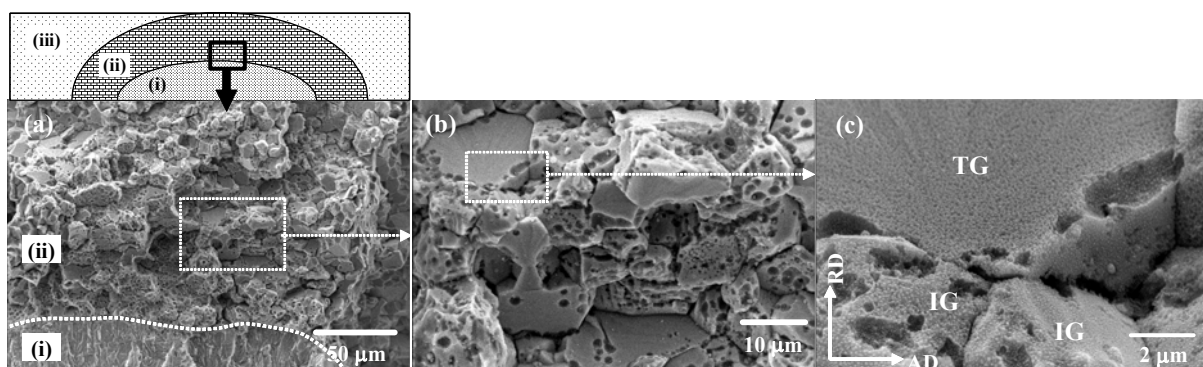


Fig. 2. Fractographs of Zircaloy-4 (RX) cladding near the interface between a pre-crack and an ISCC crack pressurized in an iodine environment at 350 °C showing transgranular (TG) and intergranular (IG) fracture; (i) Fatigued pre-crack, (ii) ISCC (iii) ductile fracture after test.

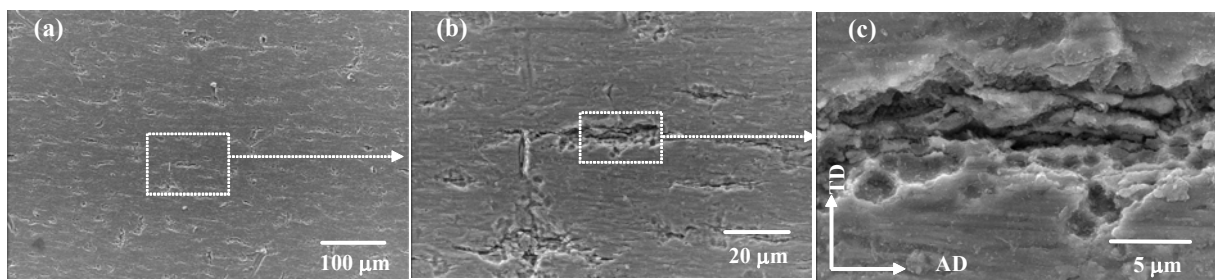


Fig. 3. Pitting morphology on the internal surface of the Zircaloy-4 cladding after an internal pressurization test at 350 °C 360 MPa for 20 hr in the iodine environment.

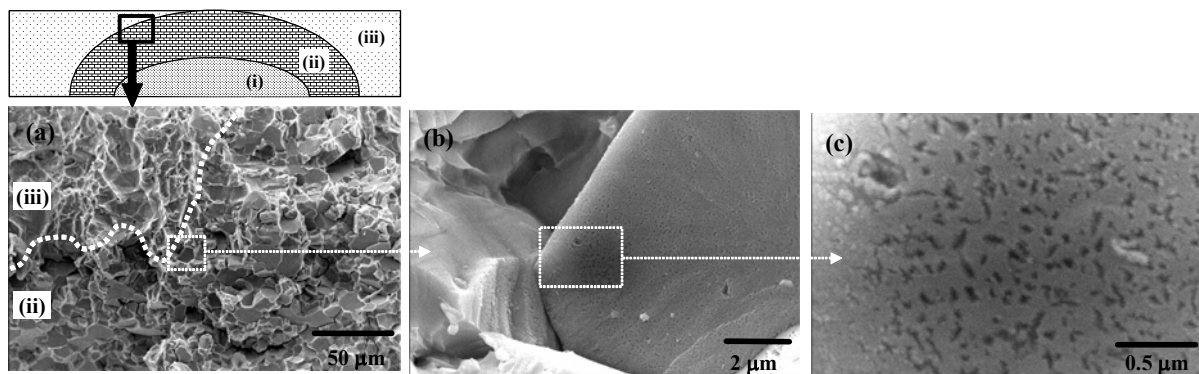


Fig. 4. Fractographs of the Zircaloy-4 (RX) cladding near the interface between the ISCC fracture and the ductile fracture pressurized in an iodine environment at 350 °C.

environment. In the early stage, the crack was propagated by intergranular (IG) cracking, in the later stage, however, it was propagated by cleavage-like transgranular (TG) cracking. And, in the intermediate stage, it was propagated with mixed mode. Fig. 2 shows SEM fractographs of the early and intermediate stage. Both IG and TG patterns were observed at the same time, showing that a lot of pits were developed on the IG surface. Regarding the TG surface, however, only a few pits were shown, to form around the GB.

Fig. 3 shows the SEM picture on the inner surface of Zircaloy-4 cladding after an internal pressurization test at 350 °C, 360 MPa for 20 h in an iodine environment. Many pits are evolved all over the inner surface of cladding. Also, many of them are agglomerated along the axial direction and they become a micro-crack. The small pits tend to coalesce into a large pit. It is observed that a fine crack evolved in the interior of a large pit.

Fig. 4 shows the fractographs of the RX Zircaloy-4 cladding near the interface between the ISCC crack and the ductile fracture (later stage of crack propagation). In this region, the only TG patterns according to cleavage and fluting were observed. And the pits of a μm scale which were observed in Fig. 2 were not observed, also. Only

small and shallow pits of nm scale were observed in the higher magnification photos (50,000X).

Fig. 5 shows the SEM images on the fractured surface of SR Zircaloy-4 cladding after the ISCC test. Fracture mode was mainly TG showing fluting and tearing.¹⁵⁾ The axially elongated microstructure inside the ISCC as well as the crack surface caused by the ISCC is clearly shown. The detailed observation on the elongated microstructure resulted that it was mainly the stress-relieved (SR) α phase. Although the pits of μm scale which were observed in Fig. 2 were not observed, very small size of pits less than

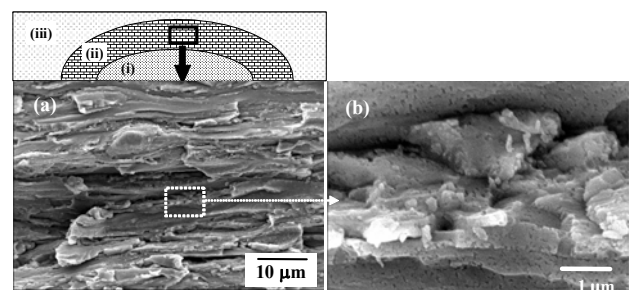


Fig. 5. Fractographs of an ISCC crack for Zircaloy-4 (SR) cladding pressurized in an iodine environment at 350 °C showing transgranular (TG) fracture.

0.05 μm were observed on the TG surface from the high magnification.

Fig. 6 shows the SEM images on the fractured surface of the SR and RX Nb-contained cladding after the ISCC test. As shown in Fig. 4(b), very small size of pits less than 0.05 μm were observed on the fracture surface.

Fig. 7 shows the effect of an alloying element on the pitting morphology and crack nucleation. Zircaloy-4 and Nb-contained Zirconium cladding were tested in the same iodine concentration for 2.6 hr and for 20 hr, respectively. Although both specimens had a number of pits and their cluster in common, their morphologies were quite different from each other. The morphology of the pitting cluster for the Nb-contained Zirconium cladding was a circular type but that for the Zircaloy-4 was elongated in the axial direction. It means that the pitting cluster of Zircaloy-4 tends to nucleate into the initial crack easier than that of Nb-contained Zirconium cladding.

Fig. 8 shows the crack propagation rate of the SR, RX Zircaloy-4 and SR Nb-contained claddings with respect to the applied K_I value. And it shows the crack propagation rate of the SR Zircaloy-4 cladding in an iodine and inert environment with respect to the applied K_I value, too. The K_{ISCC} value of the Zircaloy-4 in this study was 3.3 $\text{MPa} \cdot \text{m}^{1/2}$ and that of the Nb-contained Zirconium cladding was 4.8 $\text{MPa} \cdot \text{m}^{1/2}$, which means that the Nb-contained Zirconium cladding has a higher resistance to crack growth than that of the Zircaloy-4. The value of K_{ISCC} measured in this study was similar to other data.^{16,17)} The crack prop-

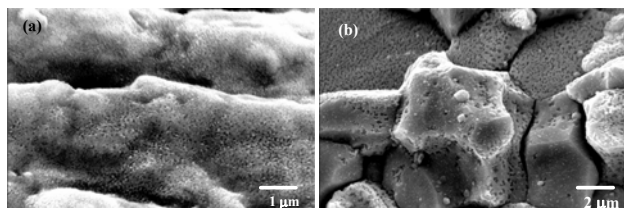


Fig. 6. Pitting morphology on the cross sectional crack surface of the Nb-contained cladding after an internal pressurization test at 350 $^{\circ}\text{C}$ in the iodine environment; (a) SR structure and (b) RX structure.

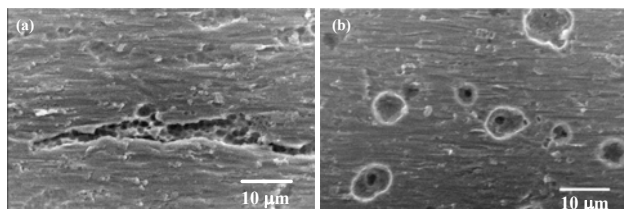


Fig. 7. Comparison of the pitting morphology between Zircaloy-4 and Nb-added cladding formed on the internal surface after an internal pressurization test at 350 $^{\circ}\text{C}$ in the iodine environment.

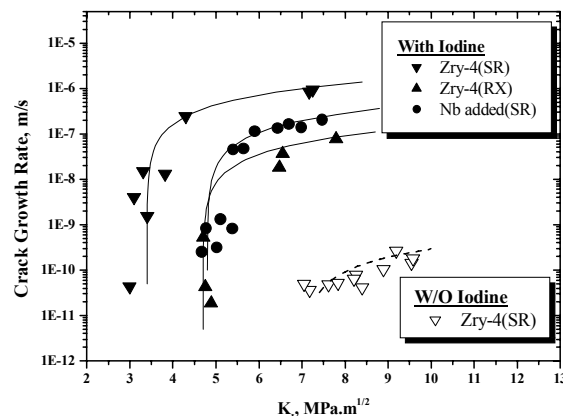


Fig. 8. da/dt vs. K_I plots for the Zircaloy-4 and Nb-contained cladding.

agation rate in region II of Zircaloy-4 was ten times higher than that of the Nb-contained Zirconium cladding. The chemical effect on the ISCC process was so large that the threshold stress intensity of the Zircaloy-4 cladding under the inert environment was increased two times and the crack propagation rate was decreased 10000 times when compared to the iodine environment.

4. Discussions

4.1 Crack initiation and propagation model

Cox³⁾ reported that the IG and TG propagation mode was a function of crack velocity and stress intensity. He reported that the ISCC crack propagates with IG mode in condition of low crack velocity and low stress intensity, while it propagates with TG mode in condition of high crack velocity and high stress intensity. The crack also propagates with the mixed IG and TG mode if the crack velocity and stress intensity are intermediate region. Fig. 1 shows change of the cracking mode for RX Zircaloy-4 from IG to TG with increase of crack depth. It means that the crack propagates along the grain boundary with very low velocity in the early stage. Fig. 2 shows SEM fractographs of the early and intermediate stage. Both IG and TG patterns were observed at the same time, showing that a lot of pits were developed on the IG surface. Regarding the TG surface, however, only a few pits were shown, to form around the GB. Fig. 2(c) shows a interface between TG and IG. It is interesting that the pits and their clusters are developed only at the bottom side of the GB. It is understood that a cleavage crack was triggered at the bottom side of the GB because the stress had been concentrated there by the arrangement of the pits with their clusters. The effect of pitting cluster on TG cracking might be similar to that of the inner surface cracking on the clad-

ding which is shown in Fig. 3.

Fig. 3 shows the inner surface of SR Zircaloy-4 cladding which was exposed to the iodine environment. In this figure, many micro-cracks were formed on the inner surface of the cladding. Many of the pits are gathered around the micro-cracks. It is seen that they coalesced into a large pitting cluster. It is understood that the corrosion is concentrated at the weak point of cladding by highly corrosive iodine and that pitting clusters play a role of nucleation sites for a crack because of the micro-cracks developed on the inner surface of the pitting clusters.

When the iodine is adsorbed into the zirconium cladding, the zirconium bond at the grain boundary (GB) will be weakened, so the surface energy will be reduced.¹⁸⁾ In addition, the free iodine can react with zirconium to form solid iodides and a gaseous zirconium tetra iodide (ZrI_4).¹⁹⁾ This gaseous ZrI_4 can be decomposed easily into the iodine at a strained surface by an applied hoop stress, thus pits are formed due to a localized attack on the GB. There are two aspects regarding the preferential attack around the GB. First, the GB will be embrittled locally because it has a large amount of impurities such as Fe, Al, Si and Cr.¹⁹⁾ Second, if a sufficient hoop stress is applied to the surface then a slip band will be formed around the GB surface thus increasing the instability.²⁰⁾ These aspects support our results as why the pitting preferentially nucleates, grows and coalescences around the GB. Such a crack initiation process may be governed by a grain-boundary pitting coalescence (GBPC). From the standpoint of the GBPC, crack initiation is not influenced by a micro-flaw inside the cladding, which is inevitably generated during the manufacturing process, but by the grain size, shape, and orientation which are mainly affected by the heat-treatment process.

It is generally known that a TG crack in Zircaloy would propagate in parallel to a basal plane.³⁾ But Peehs²¹⁾ reported that the crack would propagate easily in the 50~70 degree direction to a basal plane. Cox³⁾ also reported that a TG crack would propagate along a slippery prism plane as well as a basal plane. Zircaloy cladding of a commercial grade would be manufactured with the normal to a basal pole along the radial direction because the basal plane tends to be a habit plane for a hydride. The f_n index of the cladding specimen used in this study was 0.655. The ISCC in the cladding would propagate easily along radial direction of cladding on the prism plane. If an active crystal slip encounters a grain boundary, the grain boundary will be attacked and pitted easily by iodine because it becomes weaker. If the pitting clusters at the bottom of grain boundary get into the slip system and trigger a cleavage on the fractured surface, it could be named as a pit

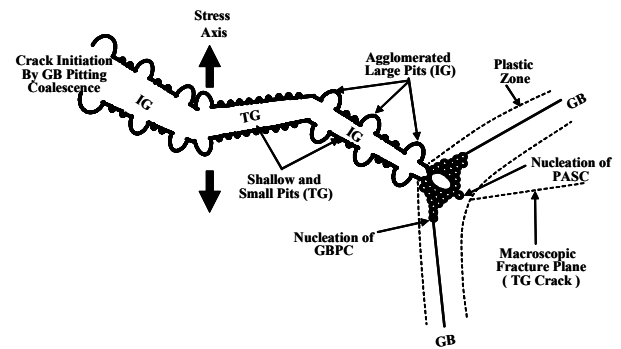


Fig. 9. Schematic diagram showing ISCC crack propagation by the grain-boundary pitting coalescence (GBPC) and pitting assisted slip cleavage (PASC) models

ting-assisted slip cleavage (PASC).

Fig. 9 shows a schematic illustration for a microcrack initiation and propagation by the GBPC and PASC models. At the GB surface of the early stage of the ISCC process, a series of reactions occurs such as a weakening of the Zr-Zr bond by the adsorbed iodine, a formation of gaseous ZrI_4 and a removal of ZrI_4 from the surface and so on, which allows the pits to grow and agglomerate in the axial direction on the GB, and an intergranular crack to grow by the GBPC process. When the crack grows to the threshold stress intensity factor, K_{ISCC} , the crack commences to propagate at a high rate by the PASC process and finally a failure takes place.

4.2 Effect of microstructure and niobium

In Fig. 5, no pit agglomerates on the fractured surface for SR Zircaloy-4. Only very small and shallow pits were formed on the whole surface. As a stress-relieved grain elongated in the axial direction and thinned in the radial one, a pitting-assisted slip cleavage (PASC) mechanism activates before a pitting agglomeration to promote crack propagation. Fig. 4 shows the interface between the ISCC fractured surface and the ductile fractured surface of the later stage of ISCC propagation for RX Zircaloy-4 cladding. In this figure, the cracking mode was almost TG due to fluting, tearing or cleavage but it shows very few pits of a μm scale which were found on the IG cracked surface in Fig. 2. However, well distributed fine pits of an nm scale can be seen in the 50,000 X SEM picture. As the depth of crack becomes deeper, the stress is concentrated on the crack tip. Thus, it seems that the PASC mechanism can be activated even at a small pitting of an nm scale. In the SR structure, a TG crack tends to propagate because the grains are elongated along the axial

Fig. 6 shows the SEM fractographs of the SR and fully recrystallized (RX) Nb-contained Zirconium cladding

which was pre-cracked and pressurized in the iodine environment. In both SR and RX structure, it was observed that a lot of small and shallow pits were developed on the whole fractured surface. Compared with the Zircaloy-4 (Fig. 2), however, pitting cluster was not found on the GB surface nor on the border of the TG. So it seems that the addition of Nb suppresses the pitting generation around the GB. Fig. 7 showed that the pitting cluster selectively formed around the GB for Zircaloy-4, whereas Nb-contained Zirconium cladding did not. In case of the pitting morphology, a circular type was found at the Nb-contained Zirconium cladding, on the other hand, micro-crack type was found at the Zircaloy-4. This implies that the Nb-contained Zirconium cladding has an equal pitting resistance both at the GB surface and the inside of a grain, whereas the pitting resistance at the GB surface is less than that at the inside of a grain in the case of Zircaloy-4.

In Fig. 8, K_{ISCC} values of the SR and RX claddings were respectively 3.3 and 4.8 MPa · m^{0.5}, which verifies that the resistance of the ISCC decreased in the SR condition. And it was revealed that the crack-propagation rate in region II of the SR microstructure was 10 times higher than that of the RX microstructure. In the early stage of a crack propagation of the RX heat-treated cladding (in Fig. 11), an intergranular fracture by a GBPC and transgranular fracture by a PASC occurred simultaneously during the cracking process, resulting in islands of transgranular fractures among lots of the intergranular fractures. In the SR heat-treated cladding, on the other hand, transgranular fractures are mainly found from the beginning of the crack propagation as shown in Fig. 5. Since the grain shape of the SR structure is a laminar type, which is elongated along the axial direction, the nm scale pits can initiate a transgranular crack on the SR cladding, and the tendency for the occurrence of transgranular cracking will be higher than that for the RX cladding. Thus, the higher possibilities of the PASC may lead to a higher crack-propagation rate for the SR cladding.

Since such GBPC and PASC mechanisms can be activated due to the corrosive characteristics of iodine, the effect of iodine on the crack propagation rate was very severe, as shown in Fig. 8. Thus, the propagation rate of the crack in the iodine environment was 10,000 times faster than that in the inert environment and the K_{ISCC} was also decreased to below one half.

5. Summary

Internal pressurization tests of the pre-cracked Zr-cladding were performed under an iodine environment. From the detailed fractographic observation, grain-boundary pit-

ting coalescence (GBPC) model and pitting-assisted slip cleavage (PASC) model were proposed for the crack initiation and propagation mechanism. This GBPC and PASC mechanisms were due to the corrosive characteristics of iodine and the effect of iodine on the crack propagation rate was very severe. The propagation rate of the crack in the iodine environment was 10,000 times faster than that in the inert environment. This model could be used to explain the ISCC resistance for SR and RX Zircaloy-4 and Nb-contained cladding.

Acknowledgments

This paper has been carried out under the Nuclear R&D program by MOST

References

1. F. Garzarolli, R. von Jan, and H. Stehle, *At. Energy Rev.* **17**, 31 (1979).
2. J. C. Wood and J. R. Kelm, *Res. Mech.*, **8**, 127 (1983).
3. J. C. Wood, *Nucl. Technol.*, **23**, 63 (1974).
4. K. Videm and L. Lunde, in: *Proc. 4th Int. Symp. On Zirconium in the Nuclear Industry*, ASTM STP-681, p.229 Stratford-upon-Avon, England, 1978.
5. D.S. Tomalin, R.B. Adamson and R.P. Gangloff, *Proc. 4th Int. Symp. On Zirconium in the Nuclear Industry*, ASTM STP-681, p.122 Stratford-upon-Avon, England, 1978.
6. R.P. Gangloff, D.E. Graham and A.W. Funkenbusch, *Corrosion*, **35**, 316 (1979).
7. B. Cox, *Proc. 4th Int. Symp. On Zirconium in the Nuclear Industry*, ASTM STP 681, p.366 Stratford-upon-Avon, England, 1978.
8. K. Videm and L. Lunde, *Proc. Am. Nucl. Soc. Topical Meeting on Water reactor Fuel Performance*, p.274, St. Charles, Ill., 1977.
9. I. Schuster, C. Lemaignan and J. Joseph, *Nucl. Eng. Design*, **156**, 343 (1995).
10. R. E. Williford, *J. Nucl. Mater.*, **132**, 52 (1985).
11. B. Cox, *J. Nucl. Mater.*, **172**, 249 (1990).
12. L.O. Jernkvist, *Nucl. Eng. Design*, **156**, 393 (1995).
13. S.Y. Park, J.H. Kim, M.H. Lee and Y.H. Jeong, *J. Nucl. Mater.*, (submitted)
14. C. Lemaignan, *Int. J. Pres. Ves. & Piping*, **15**, 241 (1984).
15. S. Shimada and M. Nagai, *J. Nucl. Mater.*, **114**, 222 (1983).
16. I. Schuster, C. Lemaignan and J. Joseph, *SMIRT-12C03/2*, 45 (1993).
17. D. Le Boulch, L. Fournier and C. S. Catherine, "Testing and Modeling Iodine-Induced Stress Corrosion Cracking in Stress Relieved Zircaloy-4", *Int. Seminar on Pellet-Cladding Interaction in Water Reactor Fuels*, Held in March 2004, Aix en Provence, France 2004.
18. B. Cox, *J. Nucl. Mater.*, **170**, 1 (1990).
19. D. Cubicciotti, R. L. Jones, B. C. Syrett, *Zirconium*

- in the Nuclear Industry*, ASTM STP 754, p.146, Boston, Mass., 1982.
20. P. Jacques, F. Lefbvre, C. Lemaignan, *J. Nucl. Mater.*, **264**, 239 (1999).
21. M. Peehs, H. Stehle and E. Steinberg, *Proc. 4th Int. Symp. On Zirconium in the Nuclear Industry*, ASTM STP-681, p.244 Stratford-upon-Avon, England, 1978.